The Elder problem - Bifurcations and steady state solutions

K. Johannsen[a]

[a]IWR/Simulation in Technology Center, Im Neuenheimer Feld 368,
69120 Heidelberg, Germany

The Elder problem is an example of a density driven flow, motivated by experiments of a thermally driven convection in porous media. It is a mathematical benchmark problem used for code verification of density driven flow simulators. We present a thorough numerical investigation of the problem on the base of the software package d^3f using a hierarchy of uniformly refined, structured grids. The bifurcation diagram with respect to the Rayleigh number is analyzed. The existence of eleven stationary solutions is shown and grid convergence is investigated numerically.

1. INTRODUCTION

Density-driven flow in porous media is relevant in a number of frequently occurring problems like saltwater intrusion, upconing phenomena and propagation of dense plumes. Several model problems have been set up to investigate the behavior analytically as well as numerically. The Elder problem and its reformulations have been designed to investigate the transient behavior of instable situations where convection is set up only by density differences. Since the early days of this problem there is an ongoing discussion which (numerically obtained) type of solution should be considered to be the "true" solution. Several grid convergence studies have been carried out to clarify this question. Up to now a satisfactory result could not be obtained. This is due to a dynamic behavior which is highly sensible to numerical perturbations, like temporal and spatial discretization errors as well as errors induced by the numerical solution schemes. It is known since the beginning of the numerical investigations that there are at least two stable steady states. Recently Frolkovic and Schepper [4] have shown the existence of a third stable, steady state. Even though this new solution has no (direct) influence on the discussion of the transient solution, it shows another aspect of the complex behavior of this model problem.

In this paper we focus on the numerical investigation of the steady state solutions. We revisit the three stable, steady state solutions found by Frolkovic and Schepper. Even though no proof on existence for this model problem is available, no reasonable doubt remains that they correspond to continuous solutions. Furthermore we show further eight steady state solutions to exist. In contrast to the three solutions known from literature these solutions are unstable in time with respect to arbitrary small perturbations. Therefore they hardly occur in the transient simulation process. Methods from the field of dynamical system are applied to derive them. The bifurcation diagram with respect to the Rayleigh number is investigated showing the interconnection of the eleven solutions.

Table 1
Parameters of the Elder problem.

Symbol	Value	Unit	Symbol	Value	Unit
n	0.1	-	ω_{max}	20%	-
D_m	$3.565 \cdot 10^{-6}$	$m^2 s^{-1}$	ρ_{min}	$1.0 \cdot 10{-}3$	kgm^{-3}
μ	10^{-3}	$kgm^{-1}s^{-1}$	ρ_{max}	$1.2 \cdot 10{-}3$	kgm^{-3}
K	$4.845 \cdot 10^{-13}$	m^2	$\|g\|$	9.81	ms^{-2}

Grid convergence is investigated in all cases. Though not directly occurring in the transient solution process, the unstable solutions may be related to the long-term unstable nonlinear behavior of the Elder problem.

The paper is organized as follows. In section 2 we briefly recall the definition of the Elder problem. Furthermore we describe the discretization method and the solution technique. Basic facts from the theory of dynamical systems are presented in section 3. We focus on a continuation method to investigate the bifurcation diagram. In section 4 numerical results are presented. Finally concluding remarks are given (section 5).

2. THE ELDER PROBLEM

The Elder problem [1,2] is an example of density driven flow where the convection is purely induced by density differences. The original thermally driven flow problem set up by Elder has been reformulated by Voss and Souza [3], among others. Here the density differences are due to heavy brine. Furthermore the geometry has been resized keeping the Rayleigh number and therefore the physical behavior unchanged.

2.1. The model problem

The governing equations for the coupled density-driven flow in porous media are derived from mass-conservation principles. Assuming incompressibility, it can be described by a system of two partial differential equations (see [5–7])

$$\frac{\partial(n\rho)}{\partial t} + \nabla \cdot (\rho v) = 0, \qquad \frac{\partial(n\rho\omega)}{\partial t} + \nabla \cdot (\rho\omega v - \rho D_m \nabla\omega) = 0, \tag{1}$$

where ω denotes the salt mass fraction, ρ the density, n the porosity, D_m the molecular diffusion coefficient and v the mass-averaged velocity given by Darcy's law

$$v = -K/\mu(\omega)(\nabla p - \rho g). \tag{2}$$

K is the permeability, μ denotes the viscosity and g the gravity vector. The Elder problem does not contain sources and sinks (vanishing right hand-side of Eqs.(1)). Furthermore dispersive effects are neglected (the diffusion in Eqs.(1) equals the molecular diffusion coefficient), permeability and viscosity are constant. The density depends on the salt mass fraction only and is given by the ideal mixing relation (see [8,6])

$$\rho^{-1} := (1 - (\omega/\omega_{max}))\, \rho_{min}^{-1} + (\omega/\omega_{max})\rho_{max}^{-1}, \tag{3}$$

where ω_{max} is the maximum salt mass fraction and ρ_{min} and ρ_{max} are the minimum and maximum density, respectively. The parameters are given in Table 1.

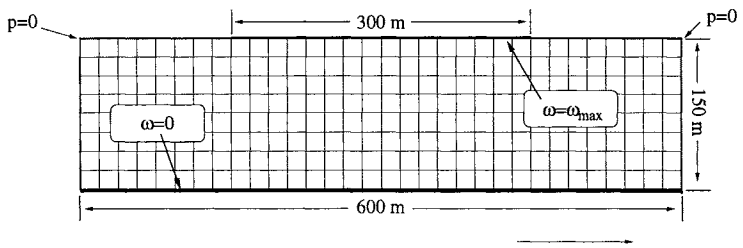

Figure 1. Elder problem: geometry, boundary conditions and coarse grid.

The geometry and boundary conditions are given in Fig. 1 together with a coarse grid. The boundary conditions indicated for ω and p are Dirichlet boundary conditions. On the other parts of the boundary no-flux boundary conditions are specified. Eqs.(1) form a differential algebraic system. Initial conditions have to be specified only for the salt mass fraction. For the Elder problem this is $\omega(x) = 0$ for $t = 0$.

Steady state solutions are obtained solving the corresponding steady state equations

$$\nabla \cdot (\rho v) = 0, \qquad \nabla \cdot (\rho \omega v - \rho D_m \nabla \omega) = 0, \tag{4}$$

arising from Eqs.(1) omitting the time derivatives. The Rayleigh number of the system is defined to be

$$Ra := [K(\rho_1 - \rho_0)|g|h] \,/\, [D_m \mu n], \tag{5}$$

where $h = 150m$ is the characteristic length of the problem. For the Elder problem we have $Ra \approx 400$.

2.2. Discretization and numerical solution

Problem (1) and (4) are solved using the program package d^3f. It uses a finite volume scheme for discretization in space. In case of problem (1), the backward Euler method is applied in time. Central differencing is applied in space leading to a non-monotonous scheme which is second-order accurate. Furthermore a consistent velocity formulation is used [11]. The non-linear discrete system of equations is solved using Newton's method. The linear subproblems are inverted applying an appropriate multigrid scheme accelerated by a Krylov subspace method. The calculations were carried out on a MIMD parallel computer using up to 32 processors. For details see [9,10].

We use square grids to perform the numerical simulations. They are derived from the coarse grid containing 4 squares by uniform refinement. In Figure 1 the grid level 3 is displayed having 297 grid points. We carried out the calculations on grid level 5 to 8 corresponding to $n_5 = 4.257$, $n_6 = 16.705$, $n_7 = 66.177$ and $n_8 = 263.425$ grid points, respectively.

3. BIFURCATIONS

In this section we consider the time evolution process of the density-driven flow to form a dynamical system and investigate its behavior with respect to the Rayleigh number. We briefly recall some basic facts from the theory of dynamical systems and focus on the generic one-parameter Fold-bifurcation. The so-called *pseudo-arclength continuation method with secant prediction* is used to calculate some solution branches connecting the different steady state solutions. Our considerations are not mathematically rigorous. E.g. the uniqueness of the time evolution of the density-driven flow equations have not been shown yet for the full set of equations we consider here. Nevertheless we claim that the results presented in section 4 are meaningful and can be made rigorous in an appropriate mathematical setting.

Following Kuznetsov [12] a *dynamical system* is a pair (φ^t, X) where X is the state space and $\varphi^t : X \to X$ the time evolution operator implicitly defined by

$$\partial_t x = f(x), \quad t \in \mathbb{R}^+. \tag{6}$$

In case of the density-driven flow model the state (ω, p) belong to $X = L_2(\Omega) \times L_2(\Omega)$ and the time evolution is given by Eqs.(1), a differential algebraic system. Eliminating p from the system it can be transformed such that it is of form (6). In the present context we are interested in the steady states of the system, i.e.

$$X_s := \{x \in X \mid \varphi^t x = x, \, \forall t \in \mathbb{R}^+\} = \{x \in X \mid f(x) = 0\}, \tag{7}$$

where $f(x) = 0$ corresponds to Eqs.(4). This set contains both stable and unstable steady states. We investigate its dependence on the Rayleigh number $Ra \in [0, 400]$. For the remainder of this section we therefore consider f to be a function of x and the Rayleigh number ($f = f(x, r)$).

Let $< \cdot, \cdot >$ be an appropriate scalar product and (x, r) be a steady state solution ($f(x, r) = 0$). Let A denote the Jacobian of Eqs.(4) with respect to x only (r fixed). Depending on A one of the two cases apply to construct new solutions $(\tilde{x}, \tilde{r})$:

- A is regular. Then there is a $\Delta r \neq 0$ such that $f(\tilde{x}, r + \Delta r) = 0$ has a unique solution in the neighborhood of x, where $r + \Delta r$ is considered to be a parameter.
- A is singular. Then there is a s with $As = 0$ and a $\delta > 0$ such that the extended system $f(\tilde{x}, \tilde{r}) = 0 \wedge < \tilde{x} - x, s >= \delta$ has a unique solution.

In the second case the system undergoes a Fold-bifurcation. In general two new steady state solutions appear varying the Rayleigh number (see Fig. 4). The result of this continuation method is a *branch* of the bifurcation diagram. It is a path in the space $X \times \mathbb{R}^+$, i.e.

$$\phi : [0, 1]_{\mathbb{R}} \to X \times \mathbb{R}^+, \quad \phi(t) = (x(t), r(t)) = ((\omega(t), p(t)), r(t)). \tag{8}$$

Every $(\omega(t), p(t))$ is a solution of Eqs.(4) with the Rayleigh number $r(t)$. We say ϕ *connects* two solutions ω_1, ω_2 if $\exists t_1, t_2 | \omega(t_1) = \omega_1 \wedge \omega(t_2) = \omega_2$. For details see [12].

In practice we apply the following

Algorithm 3.1 Set $i = 0$, choose appropriate values $\Delta r \neq 0$, $\delta > 0$ and a solution (x_0, r_0) of $f(x_0, r_0) = 0$,

1. set $r_{i+1} = r_i + \Delta r$ and solve $f(x_{i+1}, r_{i+1}) = 0$, i.e. Eqs.(4) for the changed Rayleigh number. If a solution can be found, set $i = i + 1$, repeat step 1.

2. set $s = x_i - x_{i-1}$ and solve the extended system $f(x_{i+1}, r_{i+1}) = 0 \wedge < x_{i+1} - x_i, s >= \delta$. Set $i = i + 1$. If $(r_{i+1} - r_i)(r_i - r_{i-1}) < 0$, i.e. the variation of the Rayleigh number changes sign, set $\Delta r = -\Delta r$. If sufficiently many steps 2 have been carried out, proceed with step 1, otherwise with step 2.

An adaption of the parameter δ turns out to be necessary in practice. The non-linear system to be solved in step 1 (solution of the steady state equations) is carried out as discussed before. The extended non-linear system in step 2 is solved using Newton's method. The arising linear subproblems is solved using a Schur-complement method with again involves a multigrid method accelerated by a Krylov-subspace method.

4. RESULTS

In this section we present numerical results obtained for the model problem from section 2. First we present the eleven steady state solutions (three stable, eight unstable). Then the method used to construct the solution is discussed briefly. Their interconnection in the bifurcation diagram is shown. All solutions presented in this section could be represented on every of the 4 grids (see section 2.2). If not noted otherwise the solutions shown have been obtained on grid level 8.

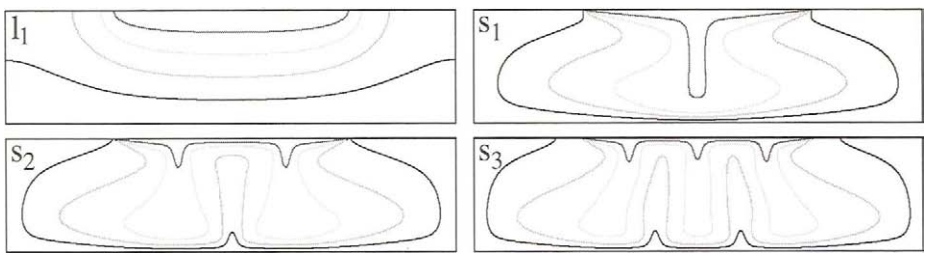

Figure 2. Elder problem: stable, steady state solutions l_1, s_1, s_2, s_3. l_1 is the unique steady state for the linear problem with $Ra = 0$, s_1, s_2, s_3 correspond to $Ra = 400$. The iso-lines correspond to the values $0.2\omega_{max}$, $0.4\omega_{max}$, $0.6\omega_{max}$ and $0.8\omega_{max}$.

The stable, steady state solutions of the Elder problem are shown in 2. Solution s_1, s_2, s_3 are the three stable, steady state solutions already found by Frolkovic and Schepper [4]. Additionally, the unique steady state l_1 of the linear Elder problem ($Ra = 0$) is presented. As we will see it is closely connected to the stable one-finger solution s_1. The eight unstable, steady state solutions are shown in Fig. 3. They have not been documented in literature yet. The labels correspond to the characteristics of the solutions: l denotes

linear, s stable, u unstable, the first (or only subscript number) denotes the number of "fingers" and the second subscript number is an enumeration index.

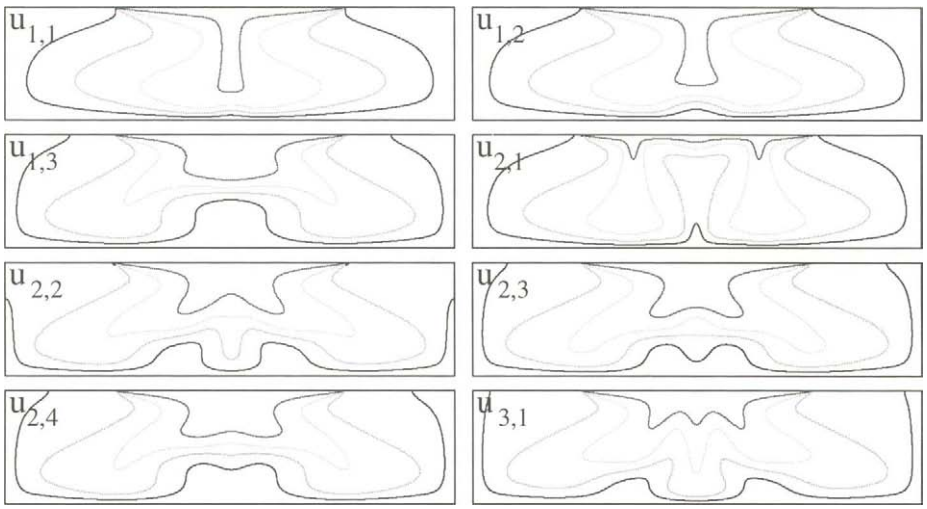

Figure 3. Elder problem: unstable, steady state solutions $u_{1,1} \ldots u_{3,1}$. The iso-lines correspond to the values $0.2\omega_{max}$, $0.4\omega_{max}$, $0.6\omega_{max}$ and $0.8\omega_{max}$.

The stable solutions s_1, s_2, s_3 can be found by a transient simulation. s_1, s_2 frequently occur in the simulation of the Elder problem. Solution s_3 can be found choosing appropriate initial conditions. The instable solutions $u_{i,j}$ have been derived using Algorithm 3.1, i.e. constructing solution branches of the Elder problem. Before going into details we show how to visualize solution branches. To this end we introduce the L_2-functional

$$L(\omega, p) := \int_\Omega \omega(x,y)\left[c_0 + c_1 f(x,300) + c_2 f(x,230) + c_3 f(x,190)\right] g(y) dxdy \tag{9}$$

with

$$\begin{aligned} f(x,x_0) = &\ \exp(-(x-x_0)^2/500) + \exp(-(x+x_0-600)^2/500), \\ g(y) = &\ 1 - 3/4(150-y)\exp((y-150)/10), \\ c_0 = &\ 1.68 \cdot 10^{-6},\ c_1 = -3.64 \cdot 10^{-4},\ c_2 = -9.57 \cdot 10^{-4},\ c_3 = 1.19 \cdot 10^{-3}. \end{aligned}$$

The integral in Eq.(9) is evaluated using a fourth order quadrature rule. To every solution (ω, p) we assign the real number $L(\omega, p)$ and a branch (8) can be displayed drawing the image of

$$\tilde{\phi} : [0,1]_{\mathbb{R}} \to \mathbb{R}^2, \quad \tilde{\phi}(s) = (L(\omega(s), p(s)), r(s)). \tag{10}$$

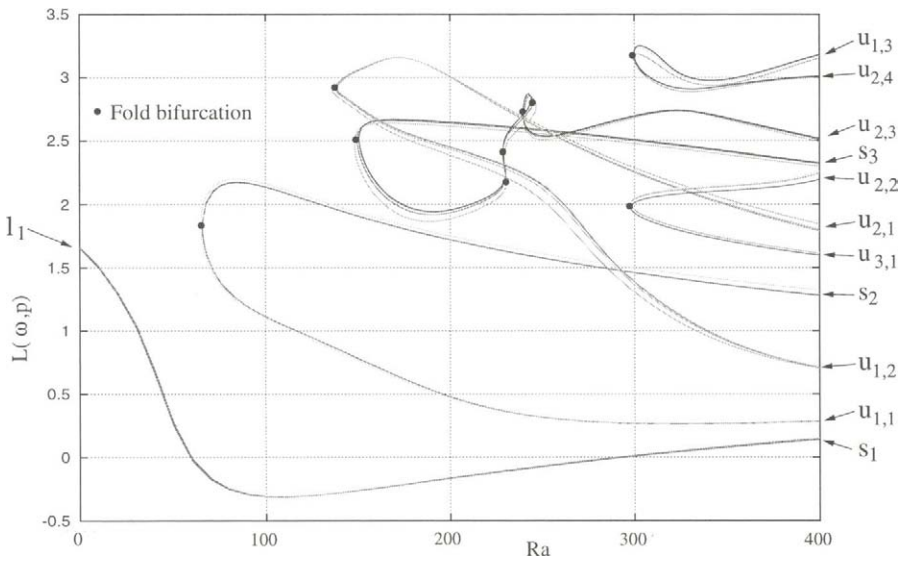

Figure 4. Solution branches of the Elder problem. The symbols correspond to the symbols in Fig. 2 and 3. Fold bifurcation points are marked with a black dot.

For the Elder problem we found six solution branches displayed in Fig. 4. The horizontal axis corresponds to the Rayleigh number, the vertical to $L(\omega, p)$. Each point in the figure represents a solution of Eqs.(4). Intersection of two branches does not mean two solutions coincide, since $L(\omega_1, p_1) = L(\omega_2, p_2)$ does not imply $(\omega_1, p_1) = (\omega_2, p_2)$.

One branch connects the stable "one-finger" solution s_1 with the linear solution l_1 ($Ra = 0$). Two of them connect stable solutions with unstable ones: s_2 with $u_{1,1}$, s_3 with $u_{2,3}$. Therefore $u_{1,1}, u_{2,3}$ can be derived from s_2, s_3 applying the path continuation method. The remaining three branches connect unstable states with unstable states: $u_{1,2}$ with $u_{2,1}$, $u_{2,2}$ with $u_{3,1}$, $u_{2,4}$ with $u_{1,3}$. They can be derived invoking non-appropriate grids being to coarse to represent the bifurcation diagram correctly. The branches break up into parts which are recombined building up a changed topology. Using interpolation between different grids one can use this changed topology to find the unstable branches.

We see that for $Ra < 65$ the Elder problem has a unique stable solution. At $Ra = 65$ the system undergoes a Fold-bifurcation and therefore we have for $65 < Ra < 136$ three solutions (two stable, one unstable) etc. Other Fold-bifurcations occur at $Ra = 138, 149, 228, \ldots$. For $(300 < Ra)$, e.g. for the original Elder problem ($Ra \equiv 400$) we have (at least) eleven solutions (three stable, eight unstable). The stability of the solutions follow from the theory of dynamical systems, numerical investigations of the transient behavior of small perturbations and spectrum analysis of the discrete Jacobian A. A detailed discussion is beyond the scope of this paper. Every of the branches displayed

in Fig. 4 is fourfold, corresponding to the grids level 5 to 8. It can be seen clearly that the topology the the bifurcation diagram does not change. Grid convergence is achieved fast for the branches connecting the solution with low spatial variations, like l_1 and s_1. It is slower for the branch connecting $u_{2,2}$ and $u_{1,3}$. Investigations not shown here using different types of triangular grids confirm these results.

5. CONCLUSIONS

We have investigated the Elder problem from the dynamical systems point of view. Applying a path continuation method we could determine new steady state solutions of the problem. Grid convergence could be achieved on a sequence of uniformly refined grids. These new solutions turn out to be unstable and therefore will never show up in a transient solution process. Nevertheless it may come close to some of these unstable states. A further investigation of these states may help to understand the long-term non-linear behavior of the transient solution.

REFERENCES

1. J.W. Elder, Steady free convection in a porous medium heated from below. J Fluid Mech 1967;27:29-48.
2. J.W. Elder, Transient convection in a porous medium. J Fluid Mech 1967;27:609-623.
3. C.I. Voss and W.R. Souza, Variable density flow and solute transport simulation of regional aquifers containing a narrow freshwater-saltwater transition zone. Water Resour Res 1987;26:2097-2106.
4. P. Frolkovic and H. De Schepper, Numerical modeling of convection dominated transport with density driven flow in porous media. Adv Water Resour 2001;24(1):63-72.
5. J. Bear and Y. Bachmat, Introduction to modeling of transport phenomena in porous media. Dordrecht: Kluwer Publ; 1991.
6. E. Holzbecher, Modeling density-driven flow in porous media. Berlin: Springer; 1998.
7. A. Leijnse, Three-dimensional modeling of coupled flow and transport in porous media. PhD thesis, University of Notre Dame, Indiana; 1992.
8. A.W. Herbert and C.P. Jackson, Lever DA. Coupled groundwater flow and solute transport with fluid density strongly dependent on concentration. Water Resour Res 1988;24:1781-1795.
9. E. Fein (ed.), d3f - Ein Programmpaket zur Modellierung von Dichtestroemungen, GRS, Braunschweig, GRS-139, ISBN 3-923875-97-5, 1998.
10. K. Johannsen, W. Kinzelbach and S.E. Oswald, Wittum G. Numerical simulation of density driven flow in porous media. Adv Water Resour 2002; to be published.
11. P. Frolkovic, Consistent velocity approximation for density driven flow and transport. In: R. Van Keer et al. editors. Advanced Computational Methods in Engineering, Part 2, Maastrich; Shaker Publishing; 1998:603-611.
12. Y.A. Kuznetsov, Elements of Applied Bifurcation Theory. Springer; 1995.